JOM, Vol. 66, No. 7, 2014
DOI: 10.1007/s11837-014-1007-y


# Progress Toward an Integration of Process–Structure–Property–Performance Models for "Three-Dimensional (3-D) Printing" of Titanium Alloys

P. C. COLLINS,[1,4] C. V. HADEN,[2] I. GHAMARIAN,[1] B. J. HAYES,[1] T. ALES,[1] G. PENSO,[1] V. DIXIT,[3] and G. HARLOW[2]

1.—Department of Materials Science and Engineering and the Center for Advanced Research and Testing, University of North Texas, Denton, TX 76203, USA. 2.—Mechanical Engineering and Mechanics, Lehigh University, Bethlehem, PA 18015, USA. 3.—*Present address:* Intel Corporation, Hillsboro, OR, USA. 4.—e-mail: peter.collins@unt.edu

Electron beam direct manufacturing, synonymously known as electron beam additive manufacturing, along with other additive "3-D printing" manufacturing processes, are receiving widespread attention as a means of producing net-shape (or near-net-shape) components, owing to potential manufacturing benefits. Yet, materials scientists know that differences in manufacturing processes often significantly influence the microstructure of even widely accepted materials and, thus, impact the properties and performance of a material in service. It is important to accelerate the understanding of the processing–structure–property relationship of materials being produced via these novel approaches in a framework that considers the performance in a statistically rigorous way. This article describes the development of a process model, the assessment of key microstructural features to be incorporated into a microstructure simulation model, a novel approach to extract a constitutive equation to predict tensile properties in Ti-6Al-4V (Ti-64), and a probabilistic approach to measure the fidelity of the property model against real data. This integrated approach will provide designers a tool to vary process parameters and understand the influence on performance, enabling design and optimization for these highly visible manufacturing approaches.

## INTRODUCTION

Since about the mid-1990s, there have existed various additive manufacturing approaches for the direct manufacture of components from structural metallic materials. While there were certainly early industrial applications that were developed to exploit the advantages of additive manufacturing, they tended to be somewhat limited or were conducted in a highly proprietary or secret fashion. Only recently have the various additive manufacturing approaches received the attention typically associated with paradigm-changing technologies. Indeed, some expect the economic output of the additive manufacturing industries to be at $3.1 billion in 2016 and $5.2 billion in 2020.[1,2] Investments being made by industry are well aligned with these projections. Thus, in the not-to-distant future, various products will be produced by additive manufacturing. Arguably, these projections of the economic impact are largely due to the benefits related to manufacturing (e.g., near-net shapes, reduced machining, higher material yield, shorter time to insertion, increased design flexibility, and increased part complexity). However, materials scientists know that manufacturing processes, at the end of the day, must manufacture a product with a material that must perform in service. It is then necessary to ask the question, "What is the effect of the novel processing on the materials performance?" The materials science community also knows that the process can have a significant influence on the microstructure and properties of a material. Thus, process development should proceed in parallel with materials development, or at the very least, an effort aimed at understanding of the

(Published online June 3, 2014)

process–structure–property–performance relationship. If additive manufacturing is going to see use in applications where performance is required, this relationship needs to be established rapidly.

To accelerate the establishment of the requisite scientific and technical understanding of these processes and (I) their influence on microstructural evolution; (II) the microstructure–property relationships; and (III) the expected statistical performance of material, a team consisting of industrial members (Boeing and Sciaky) and researchers at the University of North Texas, Lehigh University, and The Ohio State University have adopted an integrated approach. The approach seeks to provide designers a means of quantifying the confidence of a predicted property as they consider the product forms where additive manufacturing achieves an advantage (technical or economic) without an unknown risk of material or component failure during service. To accomplish this, the team is focused on the following tasks:

1. The development of a process model that will be able to predict the local thermal histories and materials compositions
2. The development of models to predict the microstructure, given a starting local composition and thermal history
3. The development of physically based strength models that incorporate composition and microstructure
4. The development of stochastic models to account for the natural probability variations that exist in a given material (database)

The specific additive manufacturing process being considered is the Sciaky electron beam, a wire-based additive manufacturing approach for large-scale structural applications. It is being applied to the widely used Ti-6Al-4V. Selected highlights of each activity are provided below, and a key linkage is demonstrated between tasks 3 and 4.

## METHODOLOGIES AND DISCUSSION

### Multiphysics Process Model

Historically, the efforts to predict the thermal history of additive manufacturing process have been the most robust modeling activities related to additive manufacturing.[3–10] The team is currently using COMSOL Multiphysics 4.3b (COMSOL, Inc., Burlington, MA), a commercially available and user-community backed multiphysics modeling and simulation software package, to predict the local thermal history for every node of the model. Some of the earliest efforts at developing finite-element models to predict the thermal history of additively manufactured components were based on the modeling of laser-based additive manufacturing of Ti-64 by S. Kelly,[6] Kelly and Kampe,[11,12] and Kobryn and colleagues.[3,13–16] Their simulations demonstrated the complex thermal histories that are expected in additively manufactured materials, where each thermal excursion is followed by a decay in temperature. In general, additive manufacturing presents some nontrivial challenges, including the basic fact that the part geometry is constantly changing as material is being added. In addition, the environment under which additive manufacturing is conducted may result in a spatially varying compositional modulation.

There are two strategies for the addition of new material in these models. The first one is to implement a scheme where new nodes can be added to the model once a condition has been satisfied, such as the time at which the heat source (and thus, new material) will be present at a given $x$–$y$–$z$ coordinate. The new nodes are added, and according to conventional finite-element strategies, the entire model is meshed (or, remeshed in this case). Obviously, this introduces a nontrivial time step that becomes increasingly burdensome for large geometries where the size of the melt pool is relatively small. The second one is based on a strategy described elsewhere,[17,18] in which the component is meshed one time only, and a number of nodes are "inactive" until the condition is met where the material would be added, at which point the nodes are "activated." A reasonable way to accomplish such activation is by modifying the thermal physical properties of the material of the inactive node so that they act as if the material described by the node is not present. For example, it is possible to set the thermal conductivity of the inactive node to be a very small fraction of the thermal conductivity of the active node (e.g., $k_{\text{inactive}} = 0.0001 \times k_{\text{active}}$). In this manner, the inactive nodes do not conduct heat away from the melt pool or component. As this wire-fed electron beam-based additive manufacturing approach is conducted under vacuum, this is a reasonable approximation and is easier to implement than powder bed based approaches. In addition, because the electron beam-based additive manufacturing process occurs under vacuum, only conduction and radiation are considered in solving for the states of heat as a function of time and location. The general heat equation, given in Eq. 1,

$$\rho C_{\text{p}} \frac{\partial T}{\partial t} + \rho C_{\text{p}} \vec{u} \cdot \nabla T = \nabla \cdot (k \nabla T) + Q \qquad (1)$$

can be solved using COMSOL, where $\rho$ is the density of the material, $C_{\text{p}}$ is the specific heat capacity at constant pressure, $\vec{u}$ is the heat flux vector, $\nabla T$ is the gradient of temperature, $k$ is the thermal conductivity, and $Q$ is the internal heat energy per unit volume added the system. For this model, the heat flux vector can be coupled with the moving heat source. The density, specific heat capacity, and thermal conductivity are functions of temperature (and composition) and are expressed in Table I.[6] Ultimately, the dependencies for composition should also be incorporated.

**Table I. Temperature dependencies of $\rho$, $C_p$, and $k$**

| Property | Phase | Temperature range, K | Polynomial |
|---|---|---|---|
| Density, kg/m$^3$ | $\alpha + \beta$ | $T \le 1268$ | $4461.1 - 0.1419*T$ |
| | $\beta$ | $1268 < T \le 1923$ | $4462.6 - 0.1425*T$ |
| | Liquid | $T > 1923$ | $5227.6 - 0.688*T$ |
| Thermal conductivity, W/(m K) | $\alpha + \beta$ | $T \le 1268$ | $1.2595 + 0.0157*T$ |
| | $\beta$ | $1268 < T \le 1923$ | $3.5127 + 0.0127*T$ |
| | Liquid | $T > 1923$ | $-12.752 + 0.024*T$ |
| Heat capacity, J/(kg K) | $\alpha + \beta$ | $T \le 1268$ | $483.04 + 0.215*T$ |
| | $\beta$ | $1268 < T \le 1923$ | $412.7 + 0.1801*T$ |
| | Liquid | $T > 1923$ | 831 |

Another complexity that arises in additively deposited material is the possibility that the composition of the additively manufactured material may exhibit fluctuations as a function of composition. This is due to two characteristics of additive manufacturing approaches. First, there can be flux of elemental species from the liquid into the vacuum (for electron beam processes, e.g., Al in Ti-6-4) or either from or to the liquid from the atmosphere for other additive manufacturing processes (e.g., laser-based under an inert gas, for example, gettering of trace oxygen from argon). Second, given the short residence time in the liquid phase and high solidification rates, there is often insufficient time for most elemental species to redistribute homogeneously within the liquid phase prior to solidification. For Ti-64, this effort is aimed at predicting the loss of aluminum to the vacuum. Fortunately, it is possible to leverage the work of Semiatin et al.,[19] who developed a general and simple modeling approach for melt losses in electron-beam, cold hearth melting operations that is readily extended to electron beam direct manufacturing (EBDM). They consider the possibility that the composition can be interface mediated (by incorporating the Langmuir equation[20]) or liquid diffusion mediated. For the details of the model, including equations for diffusivity with rational activation energies and vapor pressure, the reader is referred to the work of Semiatin et al.[19] Figure 1a and b provides snapshots of the model for a single pass for both temperature and solute variation as a function of height for a single pass. The latter shows that the aluminum varies over 200 $\mu$m. It is noted that these predicted results are early results and require validation and calibration. Nonetheless, the strategy that is being adopted in this integrated effort is clearly demonstrated. For every location in a build, it will be possible to obtain a predicted thermal profile and composition. These two variables will then be directly passed to the efforts involved in characterizing and modeling the microstructure (modeling activity 2). The composition is also a requisite input parameter to understand the material properties (modeling activity 3). The variability of the process and composition will also be used to ultimately inform the natural variability that is modeled by the stochastic models (modeling activity 4).

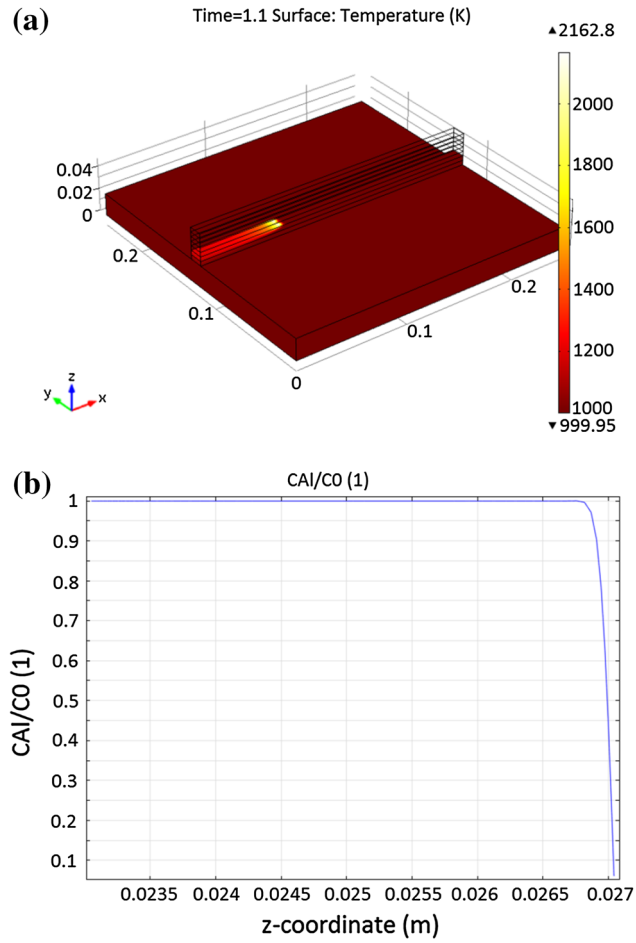


Fig. 1. Results of preliminary thermal model showing (a) the temperature distribution along the first pass and (b) the predicted aluminum concentration in a single layer due to evaporative losses from the molten pool.

## Microstructural Characterization and Modeling

Materials subject to far-from-equilibrium processing conditions or complex thermal histories,

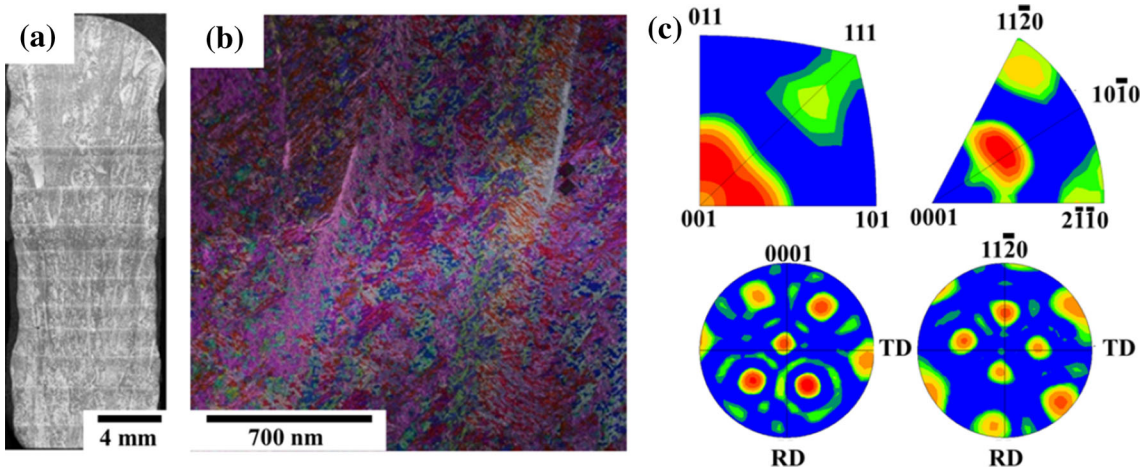


Fig. 2. Ti-64 produced via additive manufacturing. (a) Optical micrograph showing elongated vertical grains and horizontal bands of residual stress originating from the AM process. (b) Orientation map, where color and contrast correspond to orientation and residual stress, respectively. (c) Strong 001-bcc growth direction and corresponding hcp texture.

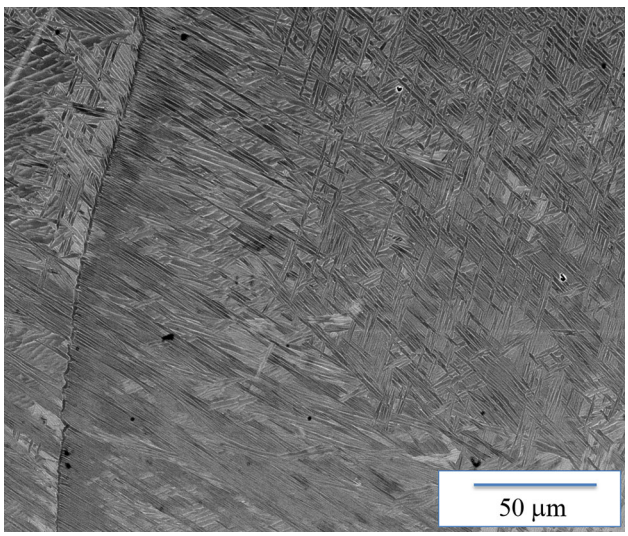


Fig. 3. Scanning electron micrograph showing the significant variation in the scale and morphology of the microstructural features within an electron beam additively manufactured Ti-64 deposit.

such as additive manufacturing, invariably contain microstructural features that are atypical when compared with conventionally processed materials. The effort underway by the team will ultimately incorporate phase-field modeling, which previously has been used to predict microstructural evolution in conventionally processed Ti-64[21–24] in order to predict the microstructure as a function of composition and local thermal history, provided by the multiphysics process model (modeling activity 1). In addition, in order to validate the phase-field models and provide a database of process–microstructure–property relationships in additive manufactured Ti-64 for subsequent extraction of constitutive predictive models for yield strength, it is necessary to accurately characterize the microstructure of the as-deposited material.

Figures 2a, c and 3 show microstructural details of Ti-64 of an electron beam additively manufactured build. In the very low magnification optical micrograph shown in Fig. 2a, it is clear that the as-deposited microstructure is highly anisotropic. There are a series of horizontal bands that are the result of residual stress, as well as elongated prior $\beta$ grains that span across multiple layer passes. The presence of the residual stress has been confirmed through both microhardness indentations within the banded structure and orientation maps (see Fig. 2b) where the color and contrast correspond to orientation and residual stress, respectively. Figure 2c shows a strong 001 body-centered cubic (bcc) $\beta$ growth direction and the corresponding hexagonal close-packed (hcp) $\alpha$ texture. Thus, in additively manufactured materials, it is reasonable to expect spatially varying composition, residual stress, and anisotropic and highly textured $\beta$ grains. In addition, the variation in the thermal history, specifically the last thermal excursion and subsequent cooling from above the $\beta$-transus, will result in different distributions of the $\alpha$-laths in the prior $\beta$ grains. The variations can be significant over a relatively small length scale. Consider Fig. 3, which shows such variation along a single prior $\beta$ grain boundary. In the top half of the micrograph, there are coarse $\alpha$-laths along the grain boundary as well as a coarse basketweave microstructure within the grains. In the bottom part of the micrograph, the $\alpha$-laths along the grain boundary are finer, and the grain interior is more colony like. In addition, it appears as if the volume fraction of the two phases is also different, although careful analysis is needed to determine whether the $\beta$ regions contain very fine-scale secondary $\alpha$-laths. These observations are consistent with spatially varying thermal history and materials composition, though the precise interrelationships have yet to be rigorously established. While the parts are ultimately subjected to a

stress-relief anneal, the starting microstructure and its variability is remembered. Although the scale of the microstructural features is coarser after heat treatment, the variation in size and type (i.e., basketweave versus colony) is retained. The quantified microstructure will be used to model the material properties (modeling activity 3). The variability of microstructure will also be used to ultimately inform the natural variability that is modeled by the stochastic models (modeling activity 4).

## Determination of a Constitutive Equation for the Prediction of Yield Strength

Ultimately, the microstructural features, including specifically the volume fraction of the $\alpha$ and $\beta$ phases, the thickness of the Widmanstätten $\alpha$-laths, the colony scale factor, the percent colony, and the thickness of the grain boundary $\alpha$ will be quantified using rigorously derived stereological procedures[25] across a wide range of specimens, resulting in a database consisting of thermal history, composition, microstructure, and properties. As the materials contain a natural distribution in the size of the features, it is necessary to develop distributions of feature sizes for inclusion in the database. This database will then be interrogated using a novel approach in which artificial neural networks have been linked with genetic algorithms to deduce a well-hidden constitutive equation for yield strength.[26]

Until quite recently, the prediction of many design properties (e.g., yield strength, ductility, fracture toughness, and fatigue) for multicomponent, multiphase engineering alloys, including specifically titanium alloys, has not been possible. This is due to the complex interrelationships that exist among composition, microstructure, and properties. As shown previously by Kar et al.[27] and Collins et al.,[28] it is quite difficult to systematically vary a single microstructural variable while keeping all others fixed at some value and thus determine the dependency of a property on a given feature. However, these efforts did demonstrate that artificial neural networks could be exercised on high-fidelity databases to capture the hidden interrelationships and unknown physics through a summation of weighted and biased hyperbolic tangent functions. In addition, these previous efforts demonstrated that it was possible to conduct virtual experiments to understand the influence of microstructure on properties. Unfortunately, the forms of the equations for yield strength that are the outcome of an optimized neural network architecture are quite complex, with forms that do not readily show the interrelationships between the compositional and microstructural details and the attending mechanical properties in any form that represents "legacy forms" (e.g., solid solution strengthening, the Hall–Petch relationship, etc.[29]). In addition, as the neural network approach is interpolative and the hyperbolic tangent functions are quite flexible, there is a risk when making predictions beyond the ranges of the database against which the optimized equation has been extracted.

The works of Ghamarian et al.[26,30] demonstrate that a new, state-of-the-art approach is possible. This approach, shown in Fig. 4, is based on the premise that the optimized flexible hyperbolic tangent functions have captured the physics and can be rewritten in an equivalent form that captures theories related to the property of interest, in this case strengthening mechanisms. Thus, this approach seeks to extract a physically based equation for yield strength that most closely approximates the complex hyperbolic tangent function deduced by the artificial neural network. To accomplish this, a database containing input variables (e.g., composition, microstructure) and outcomes (e.g., yield strength) is interrogated using artificial neural networks (labeled #1: ANN in Fig. 4), and from this a series of virtual experiments is conducted to assess the dependence of the outcome, yield strength, on the composition and microstructure. These virtual experiments then point to potential strengthening mechanisms, and a constitutive equation is postulated, based on the rather general strengthening equation given in Eq. 2

$$\sigma_{ys} = \sigma_o + \sigma_{ss} + \sigma_{ppt} + \sigma_{disp} + \sigma_{grain\ size} + \sigma_{interface} + \ldots \quad (2)$$

where $\sigma_o$ is the intrinsic flow strength of the material without any other contribution to strength, $\sigma_{SS}$ is the contribution from solid solution strengthening, $\sigma_{ppt}$ is the contribution from precipitate strengthening, $\sigma_{disp}$ is the contribution from dispersion strengthening, $\sigma_{grain\ size}$ is the contribution from grain size effects (i.e., the Hall–Petch effect), and $\sigma_{interface}$ is the contribution from interfacial strengthening. Other strengthening mechanisms, such as forest hardening, are not included in the example equation above. This equation can be appropriately modified for multicomponent and multiphase materials.[26,29] For example, based on both the virtual dependencies extracted from the artificial neural network and well-established forms of equations for strengthening mechanisms, Eq. 3 is postulated for a high-fidelity $\alpha + \beta$ wrought Ti-64 database.* In its current form, there are many unknowns. The unknowns of this equation are then optimized using genetic algorithms (labeled #2: Genetic Algorithms in Fig. 4), which iteratively solves for the solution that leads to the optimum result (see Eq. 4).

*Currently, a database for electron beam additively manufactured Ti-64 does not exist. This database is underdevelopment. To demonstrate the integration of the tool, another database has been used, and another one can be used to make predictions of strength in the $\alpha + \beta$ wrought substrate onto which the Ti-64 is additively deposited.

$$\begin{aligned}
&\sigma_{\mathrm{ys}}(\mathrm{MPa}) = (\sigma_0^{\alpha} * F_{\mathrm{V}}^{\alpha}) + (\sigma_0^{\beta} * F_{\mathrm{V}}^{\beta}) + \\
&F_{\mathrm{V}}^{\alpha} * (A_{\mathrm{Al}} * C_{\mathrm{Al}}^{n_{\mathrm{Al}}} + A_{\mathrm{O}} * C_{\mathrm{O}}^{n_{\mathrm{O}}}) + \\
&F_{\mathrm{V}}^{\beta} * ((A_{\mathrm{V}} * C_{\mathrm{V}}^{n_V})^{n_1} + (A_{\mathrm{Fe}} * C_{\mathrm{Fe}}^{n_{\mathrm{Fe}}})^{n_2})^{n_3} + \\
&k_y^{\mathrm{equiaxed_}\alpha} * F_{\mathrm{V}}^{\mathrm{equiaxed_}\alpha} * \mathrm{Equiaxed\,size}^{-n_4} + \\
&(1 - F_{\mathrm{V}}^{\mathrm{equiaxed_}\alpha}) * \frac{Colony}{100} * k_y^{\alpha_\mathrm{lath}} * (LW)^{-n_5} * (RT)^{n_5} + \\
&(1 - F_{\mathrm{V}}^{\mathrm{equiaxed_}\alpha}) * \frac{100-\mathrm{Colony}}{100} * B * \mathrm{SSS}
\end{aligned}$$

Two - phase composite of intrinsic strength
Solid - solution strengthening - hcp alpha
Potential synergistic solid - solution strengthening - bcc beta
Hall - Petch effect - Equiaxed alpha particles
Hall - Petch effect - Alpha lath
Basketweave factor

(3)

$$\begin{aligned}
&\sigma_{\mathrm{ys}}(\mathrm{MPa}) = (89 * F_{\mathrm{V}}^{\alpha}) + (45 * F_{\mathrm{V}}^{\beta}) + \\
&F_{\mathrm{V}}^{\alpha} * (149.5 * C_{\mathrm{Al}}^{0.667} + 745 * C_{\mathrm{O}}^{0.667}) + \\
&F_{\mathrm{V}}^{\beta} * ((34 * C_{\mathrm{V}}^{0.765})^{0.5} + (245 * C_{\mathrm{Fe}}^{0.765})^{0.5})^{2.15} + \\
&110 * F_{\mathrm{V}}^{\mathrm{equiaxed_}\alpha} * \mathrm{Equiaxed\,size}^{-0.5} + \\
&(1 - F_{\mathrm{V}}^{\mathrm{equiaxed_}\alpha}) * \frac{\mathrm{Colony}}{100} * 126 * (\mathrm{LW})^{-0.26} * (\mathrm{RT})^{0.26} + \\
&(1 - F_{\mathrm{V}}^{\mathrm{equiaxed_}\alpha}) * \frac{100-\mathrm{Colony}}{100} * 0.25 * \mathrm{SSS}
\end{aligned}$$

Two - phase composite of intrinsic strength
Solid - solution strengthening - hcp alpha
Potential synergistic solid - solution strengthening - bcc beta
Hall - Petch effect - Equiaxed alpha particles
Hall - Petch effect - Alpha lath
Basketweave factor

(4)

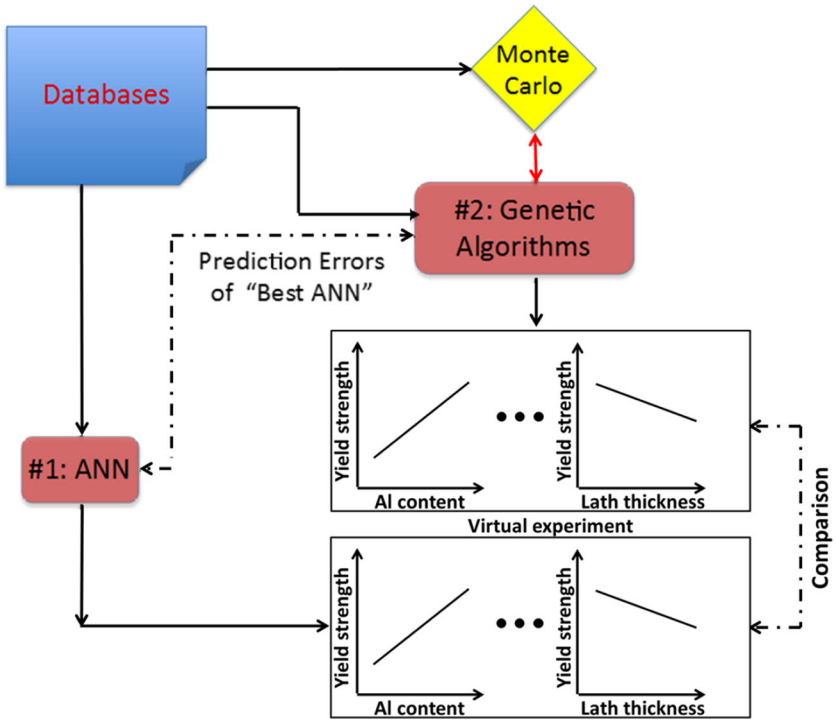


Fig. 4. The integration approach is shown. The combination of neural networks, genetic algorithm, and Monte Carlo simulation leads to deriving a phenomenological equation from a database.

Importantly, the same virtual experiments can be conducted on the optimized equation from the genetic algorithm. The premise of this hybrid artificial neural network + genetic algorithm approach is that if the virtual experiments from both the artificial neural network and the genetic algorithm closely match each other, then the constitutive equation is an approximation of the more complex equation containing a summation of weighted and biased hyperbolic tangents. Monte Carlo simulations have confirmed that, given the individual statistical uncertainties of the microstructural measurements for every data point in the database, the two equations are statistically equivalent.

The compositional and microstructural virtual dependencies determined by the artificial neural

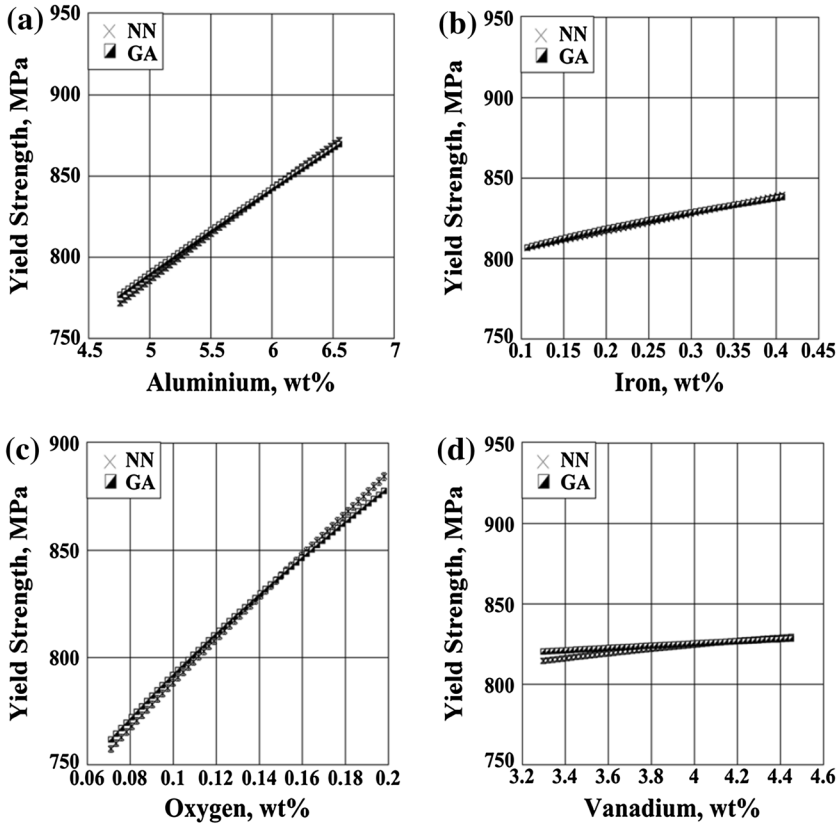


Fig. 5. Compositional virtual dependencies calculated by neural network and genetic algorithm for (a) Al, (b) Fe, (c) O, and (d) V are shown. Yield strength considerably increases by increasing the Al and O concentration. In contrast, the concentration of V has a negligible influence on yield strength.

network and genetic algorithm are given in Fig. 5a–d and 6a–d, respectively. Clearly, the predicted results using both the hyperbolic tangent functions of the neural network and the phenomenological are in very close agreement. Some of these terms, once deduced, are consistent with the limited legacy data. For example, the intrinsic strength of hcp $\alpha$ in the model is 89 MPa, which is consistent with the various literature sources on very high-purity, well-annealed titanium. Others, such as the intrinsic strength of pure bcc $\beta$, are not available in the literature. For the case of the intrinsic strength of pure bcc $\beta$, this is due to the obvious fact that it is not a thermodynamically stable at room temperature. Although currently under review, such an equation has not been presented in the literature.[26]

## Key Linkage

Although this equation is useful for a materials scientist and obviously can be directly coupled to the composition output of the process model (modeling activity 1) and the microstructures predicted by the phase-field model (modeling activity 2), it is less useful for a designer. Ultimately, a designer must know the level of confidence associated with a property, whether experimentally measured or predicted. Thus, it is important that this equation be assessed using stochastic approaches, as is shown in the next section.

## Determination of Stochastic Models to Account for Uncertainty of the Constitutive Equation for the Prediction of Yield Strength

Such constitutive equations (see Eq. 4), while challenging to deduce and thus relatively rare for real multiphase and multicomponent engineering materials, are deterministic in nature and do not account for the large variability that is known to occur naturally for each variable.[25,27] For this reason, an additional and innovative stochastic analysis was performed on the constitutive model given in the previous section. For this approach, variable states in the constitutive equation were described using the most appropriate probability distributions of Weibull, bimodal Weibull, normal, and uniform distributions to describe the inherent uncertainty in the composition and microstructure variables. The full approach is described in more detail below and allows for a confidence interval prediction on the yield stress prediction of the model. To the best of knowledge of the authors, such a confidence prediction on the predicted material strength of $\alpha/\beta$ processed Ti-6Al-4V alloys has never been produced.

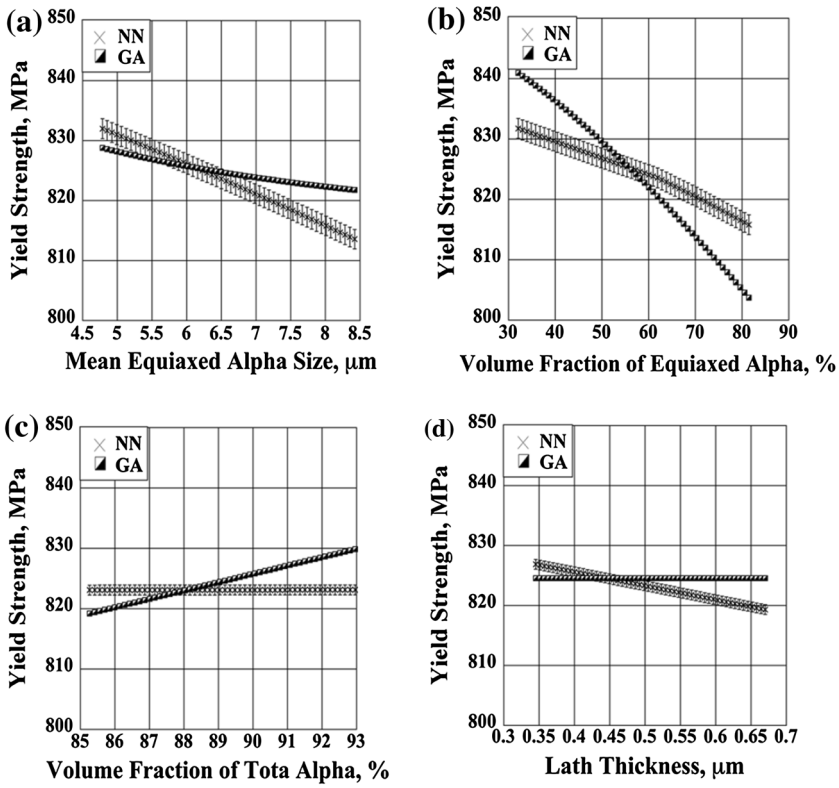


Fig. 6. Microstructural virtual dependencies calculated by neural networks and genetic algorithm for (a) mean equiaxed alpha size, (b) volume fraction of equiaxed alpha, (c) volume fraction of total alpha, and (d) lath thickness are shown.

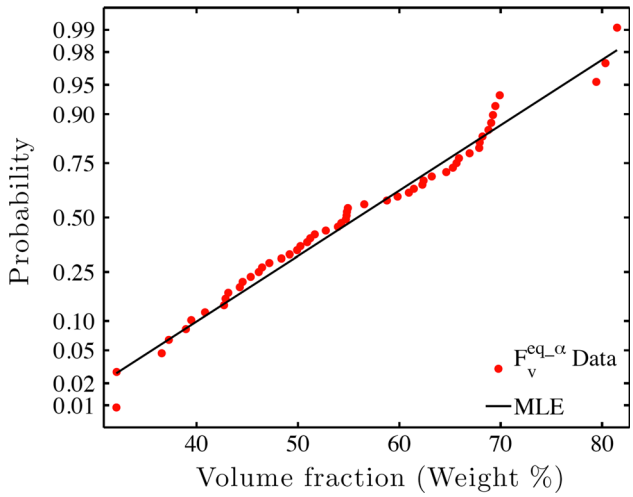


Fig. 7. Curve fit (line) and experimental data (red circles) for the volume fraction equiaxed alpha. Plotted as a normal probability.

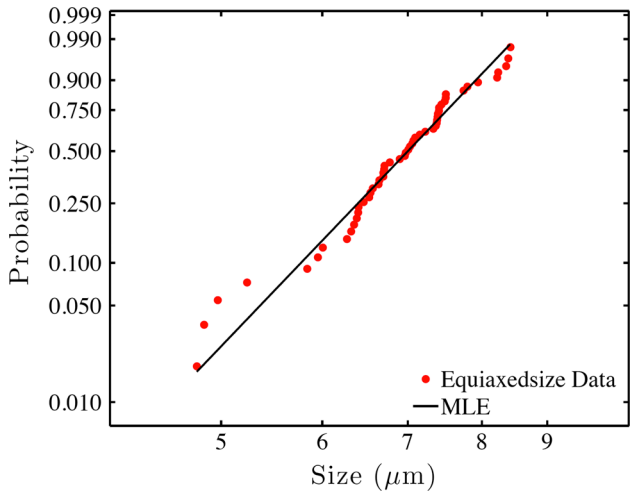


Fig. 8. Equiaxed alpha particle size data (red circles) and regression line (black line) as plotted on a Weibull probability plot.

It is necessary to first introduce the variability of the compositional and microstructural inputs. For example, the variability in material composition (composition of elements O, Fe, Al, and V) was modeled using a uniform cumulative distribution function (CDF) that was fit to the data obtained from the parameter space discussed above and based on prior literature.[31] Other distributions, including normal, Weibull, and bimodal Weibull CDFs, are potential probability distribution functions. In general, the "best" CDF can be deduced by plotting the raw data in both a normal and Weibull reference frame. The plot that results in the data being presented as a straight line is the "best" CDF (see, for example, Figs. 7 and 8). Using this approach, the volume fractions of alpha and beta particles were best approximated by normal CDFs, whereas Weibull and bimodal Weibull CDFs were

**Table II. List of all independent variables in the constitutive equation with their respective CDFs used to model their uncertainty**

| Variable name | CDF | Range | $\mu$ | $\sigma^2$ | CoV |
|---|---|---|---|---|---|
| $C_O$ | Uniform | [0.0639, 0.2718] | 0.1353 | 0.0033 | 0.4218 |
| $C_{Al}$ | Uniform | [4.284, 7.205] | 5.66 | 0.6830 | 0.1461 |
| $C_V$ | Uniform | [2.967, 4.895] | 3.84 | 0.2350 | 0.1262 |
| $C_{Fe}$ | Uniform | [0.0963, 0.4477] | 0.2522 | 0.0185 | 0.5399 |
| $F_V^{\text{total alpha}}$ | Normal | – | 90.24 | 2.8527 | 0.0187 |
| $F_V^{\text{equiaxed alpha}}$ | Normal | – | 55.24 | 152.0289 | 0.2221 |
| Equiaxed $\alpha$ size | Weibull | – | 6.9064 | 0.7189 | 0.1228 |
| Colony size | Bimodal Weibull | – | – | – | – |

Data include (when appropriate or available) the range on which these data were generated, as well as the mean, variance, and coefficient of variation for their distributions

used to estimate the equiaxed size and colony variables, respectively. These variable estimations were then used to produce a Monte Carlo simulation of the phenomenological equation described above, producing a prediction range on the yield strength calculation for the wrought $\alpha + \beta$ Ti-64. Ultimately, a similar approach will be used for electron beam additively manufactured material. While the full details will be presented soon by Collins et al.,[32] two examples of the distribution formalisms are given below. These relate to the equiaxed alpha volume fraction and particle size, distinctive features of wrought $\alpha + \beta$ Ti-64.

An assumption of normality was made for the distribution of volume fractions of the equiaxed alpha particles in the wrought $\alpha + \beta$ Ti-64. The normal distribution of the data was confirmed by the linear relationship of the volume fraction variables when plotted on normal probability paper, as shown in Fig. 7. The parameters $\mu$ and $\sigma$ for the normal CDF (Eq. 5)

$$F_x(x) = \int_{-\infty}^{x} \frac{1}{\sqrt{2\pi\sigma^2}} e^{\frac{1}{2}\left(\frac{x-\mu}{\sigma}\right)^2} dx \tag{5}$$

were estimated from the curve fit through the data (also shown in Fig. 7) according to Eqs. 6 and 7

$$\hat{\sigma} = \frac{1}{m} \tag{6}$$

$$\hat{\mu} = \frac{-b}{m} \tag{7}$$

where $m$ and $b$ are the slope and intercept of the curve fit to the data.

To simulate the volume fraction variables, the Box–Müller transform method was used to generate normally distributed random numbers between 0 and 1 ($u_N = N(0,1)$). The normal CDF was then set equal to these random numbers and solved for $x_i$ as follows (Eqs. 8 and 9):

$$F_x(x_i) = u_{N_i} \tag{8}$$

$$x_i = F^{-1}(u_{N_i}) \tag{9}$$

where $x$ represents either volume fraction variables, $F_{\mathbf{v}}^{\alpha}$ or $F_{\mathbf{v}}^{\text{eq\_}\alpha}$. The normally distributed variables of volume fraction are then simulated by the following equation (Eq. 10),

$$x_i = \hat{\sigma} \cdot u_{N_i} + \hat{\mu} \tag{10}$$

where $\hat{\sigma}$ and $\hat{\mu}$ are the estimates for the mean and the standard deviation found from the curve fit to the raw data of the volume fraction of equiaxed $\alpha$ particles.

In a similar way, it is possible to describe the Weibull probability distribution function for the equiaxed $\alpha$ particle size (see Fig. 8). The fact that the data distribution is approximately linear on this Weibull plot indicates the distribution of the equiaxed $\alpha$ particle size follows a two-parameter Weibull distribution, and it is therefore suitably modeled using such a distribution (Eq. 11).

$$F_x(x) = 1 - e^{-\left(\frac{x}{\beta}\right)^{\alpha}} \tag{11}$$

where the parameters $\alpha$ and $\beta$ are approximated by the curve fit through the data as shown in Fig. 8 and according to the following equations (Eqs. 12 and 13)

$$\hat{\alpha} = m \tag{12}$$

$$\hat{\beta} = e^{\frac{-b}{\alpha}} \tag{13}$$

To simulate a Weibull distribution for the equiaxed $\alpha$ particle size variable, the two-parameter Weibull CDF (Eq. 11) was then set equal to uniformly distributed random numbers and solved for $x$, as given below (Eqs. 14 and 15).

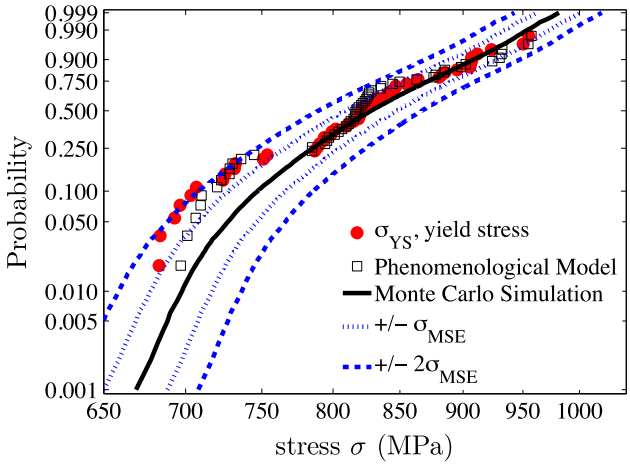


Fig. 9. Probability of experimental yield strength data (red circles) compared with the constitutive model prediction (black squares) and Monte Carlo simulations (black line). A confidence interval of one and two standard deviations is also shown (blue dashed lines).

$$F_x(x_i) = u_i \tag{14}$$

$$x_i = F^{-1}(u_i) \tag{15}$$

where $u$ = U(0,1). Similar approaches were taken for the other microstructural variables.

Table II summarizes the list of nine variables simulated for use in the constitutive equation given in the previous section.

The type of cumulative frequency distribution used to represent each variable is shown, as well as the range, mean, variance, and coefficient of variation for their distributions when appropriate.

The variables defined above were used to produce a Monte Carlo simulation of the yield stress using Eq. 4. As seen in Fig. 9, the distribution of the experimental data obtained for the yield strength correspond well to the simulated values in the upper range, above approximately 780 MPa. A bifurcation from the simulation values in the lower regime indicates a possible bimodal distribution in these data. Fortunately, the Monte Carlo simulation allows the prediction of a confidence interval around the predicted values of yield stress, with one and two standard deviations shown in blue. As seen in this figure, the data lay closely within this confidence interval, except for a few data around 700 MPa, a relatively low yield point for Ti-64.

Further refinement of the stochastic model will be possible with a wider range of parameters once they become available. However, this first approximation on the yield strength of wrought $\alpha + \beta$ Ti-6-4 alloys is valuable in drawing a confidence range on the complex relationship between the variables and output generated by the phenomenological equation (Eq. 1).

### State of the Art

As noted in the text, the establishment of a constitutive equation for the prediction of tensile properties given a certain composition/microstructure and the assessment of the uncertainty of the predictions represent the current state of the art. Rarely are such constitutive equations produced for multicomponent and multiphase engineering alloys. When such equations do exist, invariably they lack an assessment of the quality of the equations/model. In principle, the stochastic modeling approach provides an initial method of validating the constitutive equations and gives an assessment of "confidence" associated with an equation. The distributions of both the predicted data and experimentally measured data should be equivalent. However, these are for well-populated data sets. Thus, in practice for the foreseeable future, there remains the need to apply these predictive tools to materials that are not part of the original database. Only then will there be true confidence in the validation efforts. As applied here for EBDM, the efforts are to validate the models. Once validated, these new methods promise to shorten the development cycle and ultimately result in fewer tests being conducted when assessing such new manufacturing approaches.

## CONCLUSION

As this article is presented as an integrated effort to develop and couple process, structure, property, and performance models of electron beam additive (or direct) manufacturing, the conclusions are presented as "the path forward." It summarizes where the team efforts are, as well as discusses some next steps.

### The Path Forward

The various activities, as described above, each contains breakthroughs that have not yet been presented in the literature. While many are working on developing thermal modeling for additive manufacturing, the authors are not aware of any who have integrated a means of predicting variation in the solute content within the part, which will ultimately significantly impact the local properties, as shown by the constitutive equation (Eq. 4). Additionally, efforts are underway to accelerate the process model. New techniques based on spectral or fast Fourier transform (FFT)-based finite element modeling (FEM) models offer a potentially attractive means to accomplish such acceleration. The characterization clearly points to a significant spatial variation in the as-deposited microstructure, along with spatially varying residual stress. These variations will be better understood by coupling in phase-field modeling. The spatial variation will ultimately be quantified and will be a key input in

this integrated strategy. Among the most exciting developments of this program are the provision of a modeling strategy to deduce a well-hidden constitutive equation of a property (e.g., yield strength) and the subsequent interrogation of the constitutive equation against a database to understand how well it predicts the given property, given the natural variation that occurs for each compositional and microstructural variable. Such an integration has not been presented for structural titanium alloys. However, it is a means of providing a statistical framework for subsequent uncertainty analysis, which is important for the designer and provides the "E" in ICME (Integrated Computational Materials Engineering). While this initial effort to extract a constitutive equation and model its predictive ability using stochastic models has been demonstrated for wrought $\alpha + \beta$ Ti-64, it is expected to be particularly well suited for an additively manufactured electron beam which exhibits natural variations in both composition and microstructure that should be quantified. It is important to also consider what is missing from this integrated strategy. This current strategy does not seek to understand the physics associated with solidification process, although it is obvious that such an effort is ultimately needed for a broader understanding of additive manufacturing. In addition, this approach does not include a cost model, which would also be a requisite tool for end users.

## ACKNOWLEDGEMENTS

The authors gratefully acknowledge the support of DARPA Contract HR0011-12-C-0035, "An Open Manufacturing Environment for Titanium Fabrication," the support of Boeing Research and Technology and the technical lead (David Bowden), Sciaky, and The Ohio State University. In addition, the authors are grateful to Lehigh University, the University of North Texas, and UNT's Center for Advanced Research and Technology (CART).

## REFERENCES

1. T.T. Wohlers, *Wohlers Report* (2013).
2. T.T. Wohlers, *Wohlers Report* (2010).
3. P. Kobryn and S. Semiatin, *J. Mater. Process. Technol.* 135, 330 (2003).
4. P. Kobryn and S. Semiatin, *JOM* 53, 40 (2001).
5. S. Kelly, S. Babu, S. David, T. Zacharia, and S. Kampe, *Cost-Affordable Titanium: Symposium Dedicated to Professor Harvey Flower*, ed. F.H. Froes, M.A. Imam, and D. Fray (Warrendale, PA: TMS, 2004), pp. 45–52.
6. S.M. Kelly (Master's thesis, Virginia Polytechnic Institute and State University, 2002).
7. K.T. Makiewicz (Ph.D. Dissertation, The Ohio State University, 2013).
8. B. Vrancken, L. Thijs, J.-P. Kruth, and J. Van Humbeeck, *J. Alloys Compd.* 541, 177 (2012).
9. C. Charles (Licentiate Thesis, Luleå University of Technology, 2008).
10. N. Shen and Y. Chou, *23rd Annual International Solid Freeform Fabrication Symposium*, ed. D.L. Bourell (Austin, TX: University of Texas at Austin, 2012), pp. 774–784.
11. S. Kelly and S. Kampe, *Metall. Mater. Trans. A* 35, 1861 (2004).
12. S. Kelly and S. Kampe, *Metall. Mater. Trans. A* 35, 1869 (2004).
13. S. Bontha, N.W. Klingbeil, P.A. Kobryn, and H.L. Fraser, *J. Mater. Process. Technol.* 178, 135 (2006).
14. S. Semiatin, P. Kobryn, E. Roush, D. Furrer, T. Howson, R. Boyer, and D. Chellman, *Metall. Mater. Trans. A* 32, 1801 (2001).
15. E. Roush, P. Kobryn, and S. Semiatin, *Scr. Mater.* 45, 717 (2001).
16. S. Bontha, N.W. Klingbeil, P.A. Kobryn, and H.L. Fraser, *Mater. Sci. Eng. A* 513, 311 (2009).
17. H. Conrad, T. Klose, T. Sandner, D. Jung, H. Schenk, and H. Lakner, *Proceedings of COMSOL Conference* (Hannover, Germany, 2008).
18. P. Michaleris, private communication, 2013.
19. S. Semiatin, V. Ivanchenko, and O. Ivasishin, *Metall. Mater. Trans. B* 35, 235 (2004).
20. I. Langmuir, *Phys. Rev.* 2, 329 (1913).
21. Q. Chen, N. Ma, K. Wu, and Y. Wang, *Scr. Mater.* 50, 471 (2004).
22. F. Zhang, S.-L. Chen, Y. Chang, N. Ma, Y. Wang, and J. Phase, *Equilib. Diffus.* 28, 115 (2007).
23. R. Shi, N. Ma, and Y. Wang, *Acta Mater.* 60, 4172 (2012).
24. R. Shi, V. Dixit, H.L. Fraser, and Y. Wang, *Acta Mater.* (accepted for publication, 2014).
25. P. Collins, B. Welk, T. Searles, J. Tiley, J. Russ, and H. Fraser, *Mater. Sci. Eng. A* 508, 174 (2009).
26. I. Ghamarian, P. Samimi, V. Dixit, and P.C. Collins, *Metall. Mater. Trans. A* (submitted for publication).
27. S. Kar, T. Searles, E. Lee, G. Viswanathan, H. Fraser, J. Tiley, and R. Banerjee, *Metall. Mater. Trans. A* 37, 559 (2006).
28. P.C. Collins, S. Koduri, B. Welk, J. Tiley, and H.L. Fraser, *Metall. Mater. Trans. A* 44, 1441 (2013).
29. P.C. Collins and H.L. Fraser, *ASM Handb.* 22A, 377 (2009).
30. I. Ghamarian (Master thesis, University of North Texas, 2012).
31. W. Nicholson, *Biometrika* 57, 273 (1970).
32. P.C. Collins, C.V. Haden, and D.G. Harlow, unpublished research, 2014.